SHORT REPORT

Figures and figure supplements

The Axin scaffold protects the kinase GSK3β from cross-pathway inhibition

Maire Gavagan *et al*.

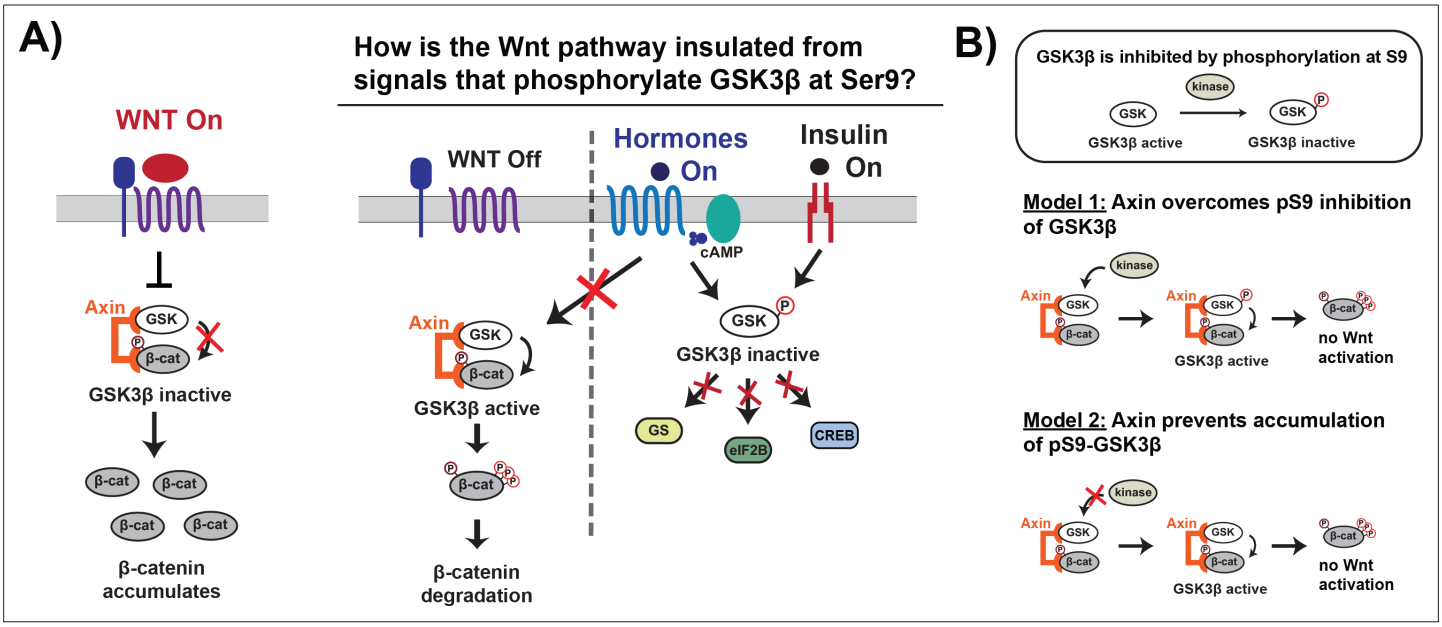

Figure 1. Wnt signaling is insulated from signals that phosphorylate GSK3β at Ser9. (**A**) In the Wnt pathway, the scaffold protein Axin coordinates a GSK3β complex that phosphorylates β-catenin, which is then degraded. Wnt signals inhibit phosphorylation, allowing β-catenin levels to rise and initiate a transcriptional program (***Nusse and Clevers, 2017***). In other signaling pathways, upstream signals regulate GSK3β through phosphorylation at Ser9, which blocks substrate binding, inhibits activity toward downstream substrates, and activates downstream signaling (***Sutherland, 2011***). (**B**) The scaffold protein Axin could insulate Wnt-associated GSK3β from Ser9 inhibition by restoring GSK3β activity toward β-catenin even when phosphorylated at Ser9 (Model 1) or by preventing accumulation of pS9-GSK3β in the Wnt destruction complex (Model 2).

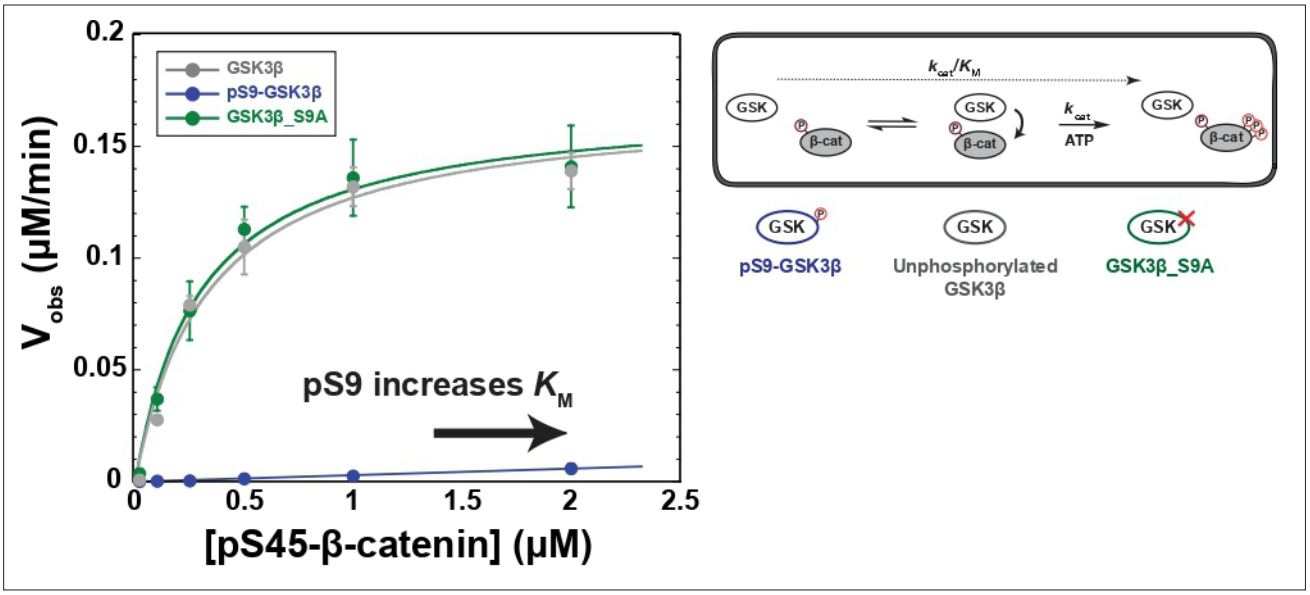

Figure 2. Phosphorylation at Ser9 inhibits GSK3β activity toward pS45-β-catenin. Kinetic scheme and Michaelis-Menten plots for reactions of unphosphorylated GSK3β, pS9-GSK3β, and GSK3β_S9A with pS45-β-catenin. Plots are V_{obs} versus [pS45-β-catenin] at 10 nM GSK3β. GSK3β phosphorylates pS45-β-catenin at three sites: S33, S37, and T41. Values are mean ± SD for at least three biological replicates. See ***Supplementary file 1a*** for values of fitted kinetic parameters. See ***Figure 2—figure supplement 1C and D*** and ***Figure 2—figure supplement 9*** for characterization of GSK3β phosphorylation states and mutants.

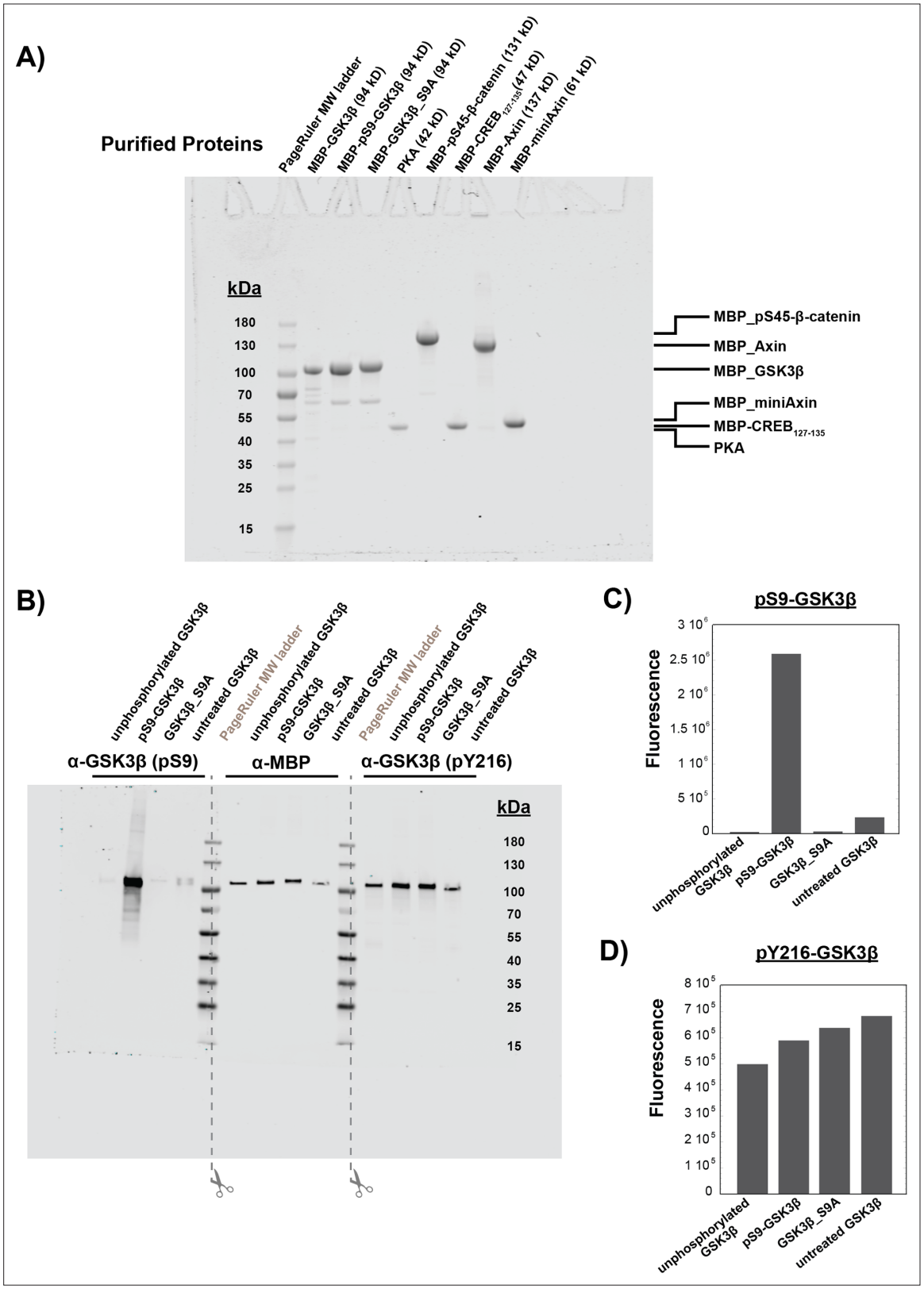

Figure 2—figure supplement 1. Characterization of purified proteins. (**A**) Coomassie-stained SDS-PAGE of purified proteins used in this work. All proteins except PKA were purified as MBP fusion proteins (see Materials and methods). Unphosphorylated GSK3β was purified after coexpression with lambda phosphatase (see Methods). pS45-β-catenin was purified after coexpression with CK1α as described previously (***Gavagan et al., 2020***). Phosphorylated GSK3β and GSK3β_S9A were purified after in vitro phosphorylation with PKA (see Materials and methods). Each lane was loaded with

Figure 2—figure supplement 1 continued on next page

Figure 2—figure supplement 1 continued

10 μL of 4 μM protein. (**B**) Western blot for phosphorylation state of GSK3β at Ser9 and Tyr216. GSK3β samples are unphosphorylated GSK3β, pS9-GSK3β, GSK3β_S9A, and untreated GSK3β (unmodified recombinant protein, not coexpressed with lambda phosphatase or treated with PKA). After the western blot transfer, the membrane was cut down the center of the MW ladder lanes so each third of the membrane could be incubated with separate antibodies (α-pS9-GSK3β, α-MBP for total protein, and α-pY216-GSK3β). The membrane fragments were placed back together for imaging. (**C**) PKA phosphorylates GSK3β at Ser9. The extent of Ser9 phosphorylation was quantified by western blot (B). Fluorescence values were normalized using the α-MBP total protein loading control. No significant phosphorylation at Ser9 was detected for unphosphorylated GSK3β (phosphatase-treated) or GSK3β_S9A. Untreated GSK3β is partially (~10%) phosphorylated at Ser9. (**D**) Recombinant GSK3β is phosphorylated at Tyr216. The extent of Tyr216 phosphorylation was quantified by western blot (B). Fluorescence values were normalized using the α-MBP total protein loading control.

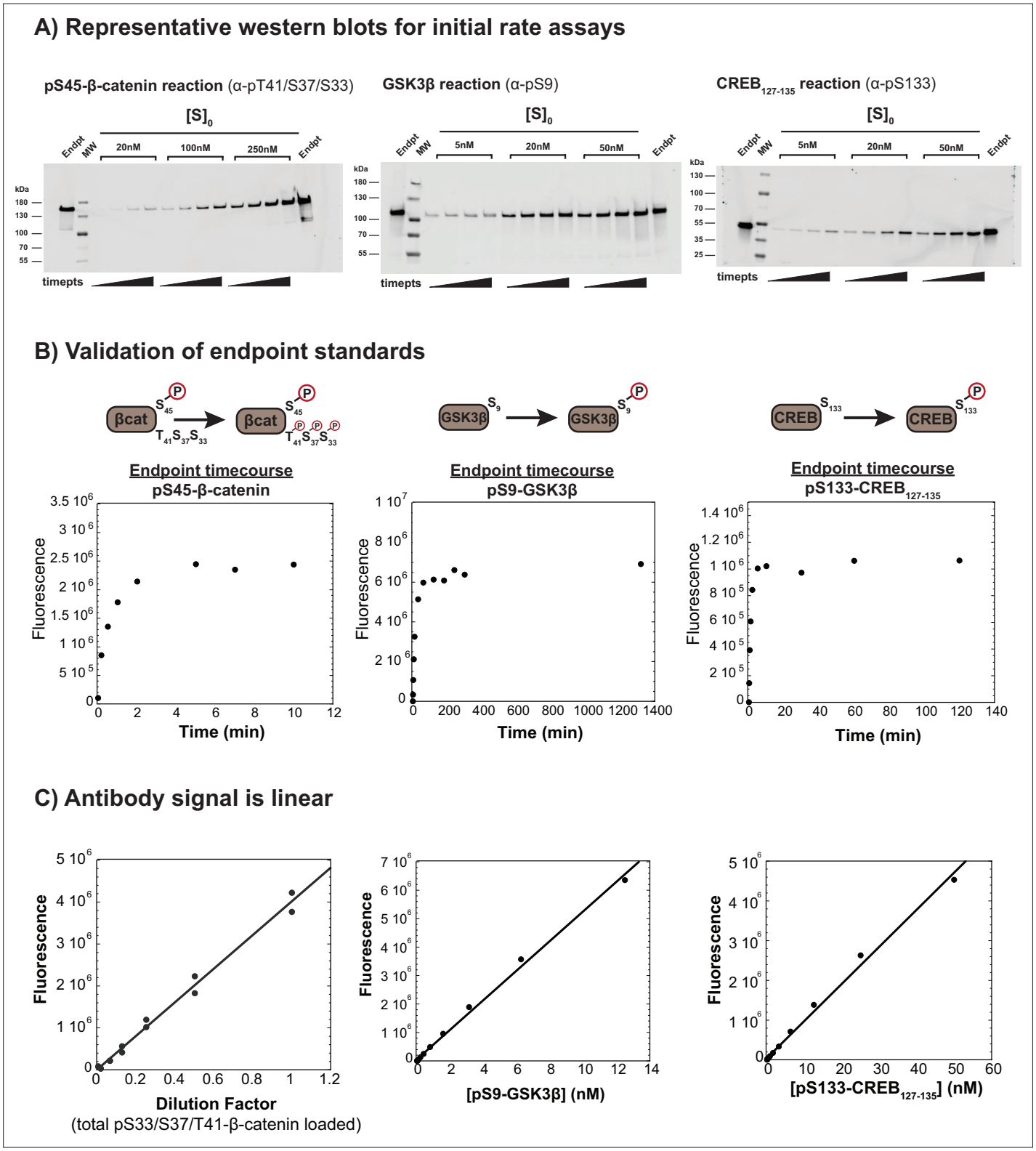

Figure 2—figure supplement 2. Protein phosphorylation kinetic assays. (**A**) Representative western blots for reactions of GSK3β with pS45-β-catenin, PKA with GSK3β, and PKA with $CREB_{127-135}$. Reactions were conducted with 10 nM GSK3β or 20 nM PKA and the substrate concentrations indicated. Each gel was cut before transferring to the membrane to facilitate multiple simultaneous transfers in the same apparatus (as seen in ***Figure 2—figure supplement 4***, ***Figure 2—figure supplement 6***, and ***Figure 4—figure supplement 1***). The images shown are the complete, uncropped blot membrane images. (**B**) Timecourses of phosphorylation of endpoint standards for GSK3β-phosphorylated pS33/pS37/pT41-β-catenin, PKA-

Figure 2—figure supplement 2 continued on next page

Figure 2—figure supplement 2 continued

phosphorylated pS9-GSK3β, and PKA-phosphorylated pS133-CREB$_{127-135}$. (**C**) The antibody signals are linear over a broad range spanning the observed signal in kinetic assays. The pS33/pS37/pT41-β-catenin data shows serial dilutions from a reaction timepoint with 3 μM pS45-β-catenin, 20 nM GSK3β and 500 nM miniAxin. The reaction was quenched at 1.5 min, which produces ~500 nM pS33/pS37/pT41-β-catenin. The quenched timepoint was diluted 1:5, then a set of twofold serial dilutions was loaded on the gel. The signal is linear over a concentration range of at least 1.5–100 nM. These data were published previously (***Gavagan et al., 2020***). The pS9-GSK3β and pS133-CREB127-135 plots show sets of twofold serial dilutions from a 1:4 dilution of pS9-GSK3β endpoint (PKA reactions with GSK3β) or undiluted endpoint (PKA reactions with CREB127-135), respectively. The pS9-GSK3β signal is linear over a range of at least 0.2–12.5 nM. The CREB127-135 signal is linear over a range of at least 1–50 nM.

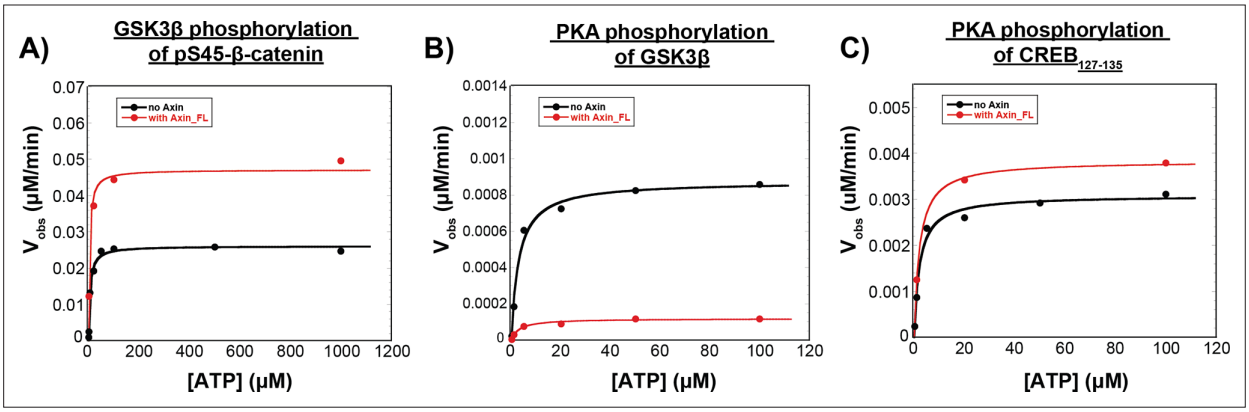

Figure 2—figure supplement 3. The concentration of ATP used for quantitative kinetic experiments (100 μM) is saturating for all reactions. (**A**) Michaelis-Menten plot of V_{obs} vs. [ATP] at 10 nM unphosphorylated GSK3β and 50 nM pS45-β-catenin in the presence and absence of 500 nM Axin. Fits to the Michaelis-Menten equation give $K_{M,\ ATP}$ values of 4.6±0.9 μM and 3.7±1.3 μM in the presence and absence of Axin, respectively. (**B**) Michaelis-Menten plot of V_{obs} vs. [ATP] at 20 nM PKA and 20 nM GSK3β in the presence and absence of 500 nM Axin. Fits to the Michaelis-Menten equation give $K_{M,\ ATP}$ values of 3.0±0.6 μM and 3.3±0.8 μM in the presence and absence of Axin, respectively. (**C**) Michaelis-Menten plot of V_{obs} vs. [ATP] at 20 nM PKA and 20 nM $CREB_{127\text{-}135}$ in the presence and absence of 500 nM Axin. Fits to the Michaelis-Menten equation give $K_{M,\ ATP}$ values of 2.1±0.4 μM and 2.1±0.2 μM in the presence and absence of Axin, respectively. K_M values for (**A**)-(**C**) are compiled in ***Supplementary file 1c***.

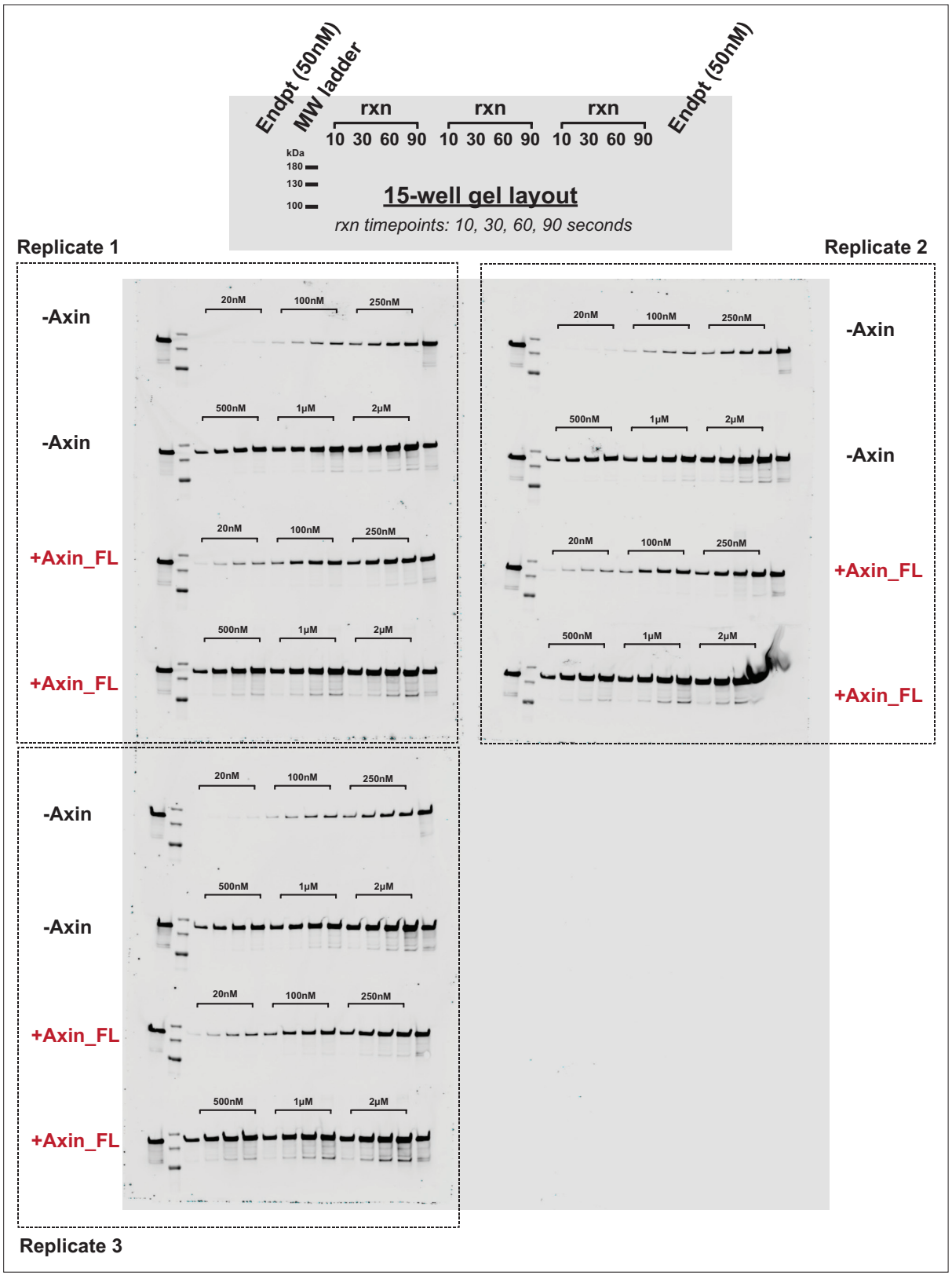

Figure 2—figure supplement 4. Representative western blots for the reaction of unphosphorylated GSK3β with pS45-β-catenin in the presence and absence of Axin. Western blots for reactions of varying concentrations of pS45-β-catenin with 10 nM GSK3β in the presence and absence of 500 nM Axin. All gel samples were diluted 1:5 to prevent a gel smearing artifact (see Materials and methods). See ***Figure 2—figure supplement 5*** for quantification.

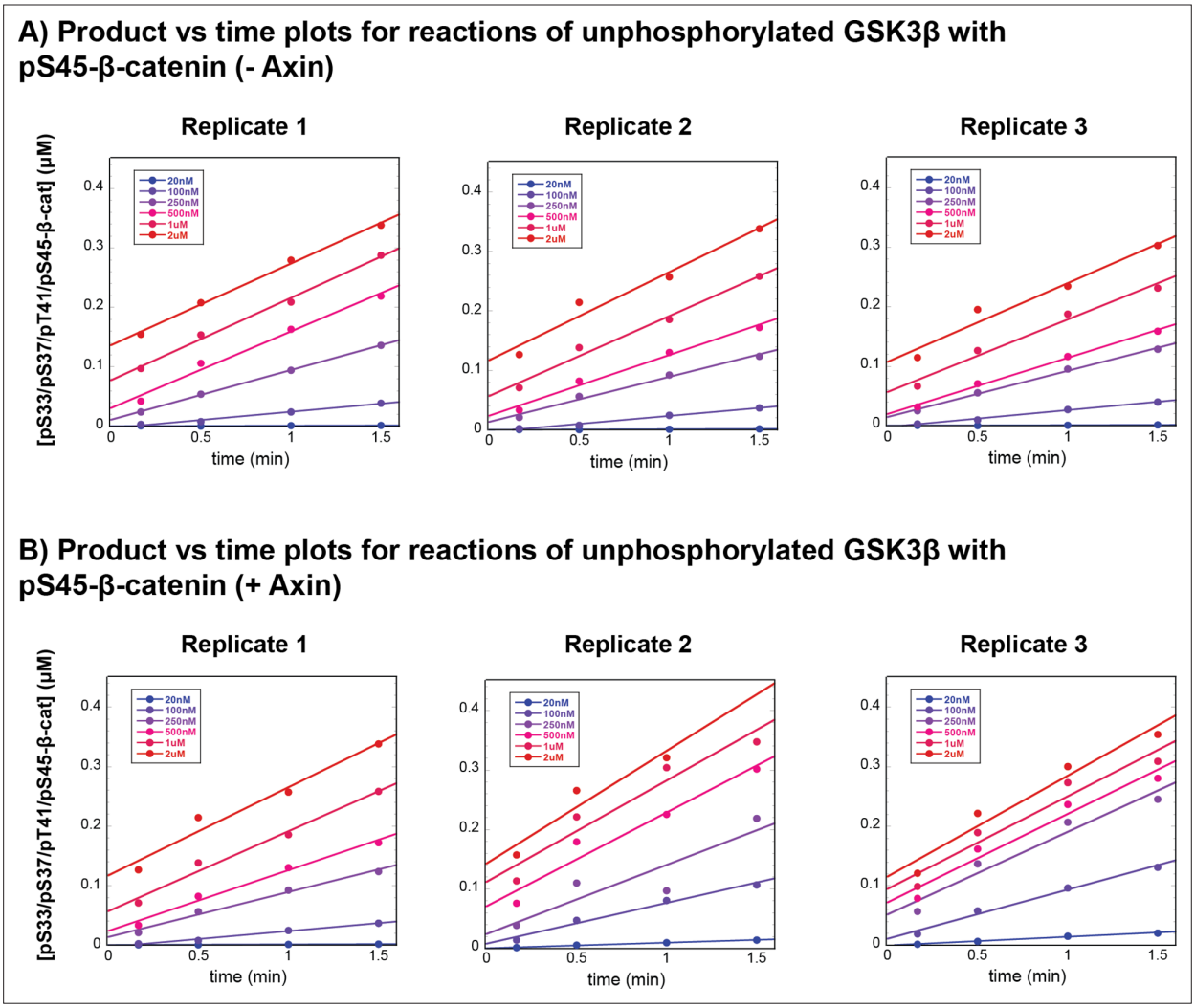

Figure 2—figure supplement 5. Plots of product vs. time for reaction of GSK3β with pS45-β-catenin in the presence and absence of Axin. (**A**) Product vs. time plots for reactions of unphosphorylated GSK3β with pS45-β-catenin in the absence of Axin. (**B**) Product vs. time plots for reactions of GSK3β with pS45-β-catenin in the presence of 500 nM Axin. Data in (**A**) and (**B**) correspond to the reaction conditions and western blots shown in ***Figure 2—figure supplement 4***.

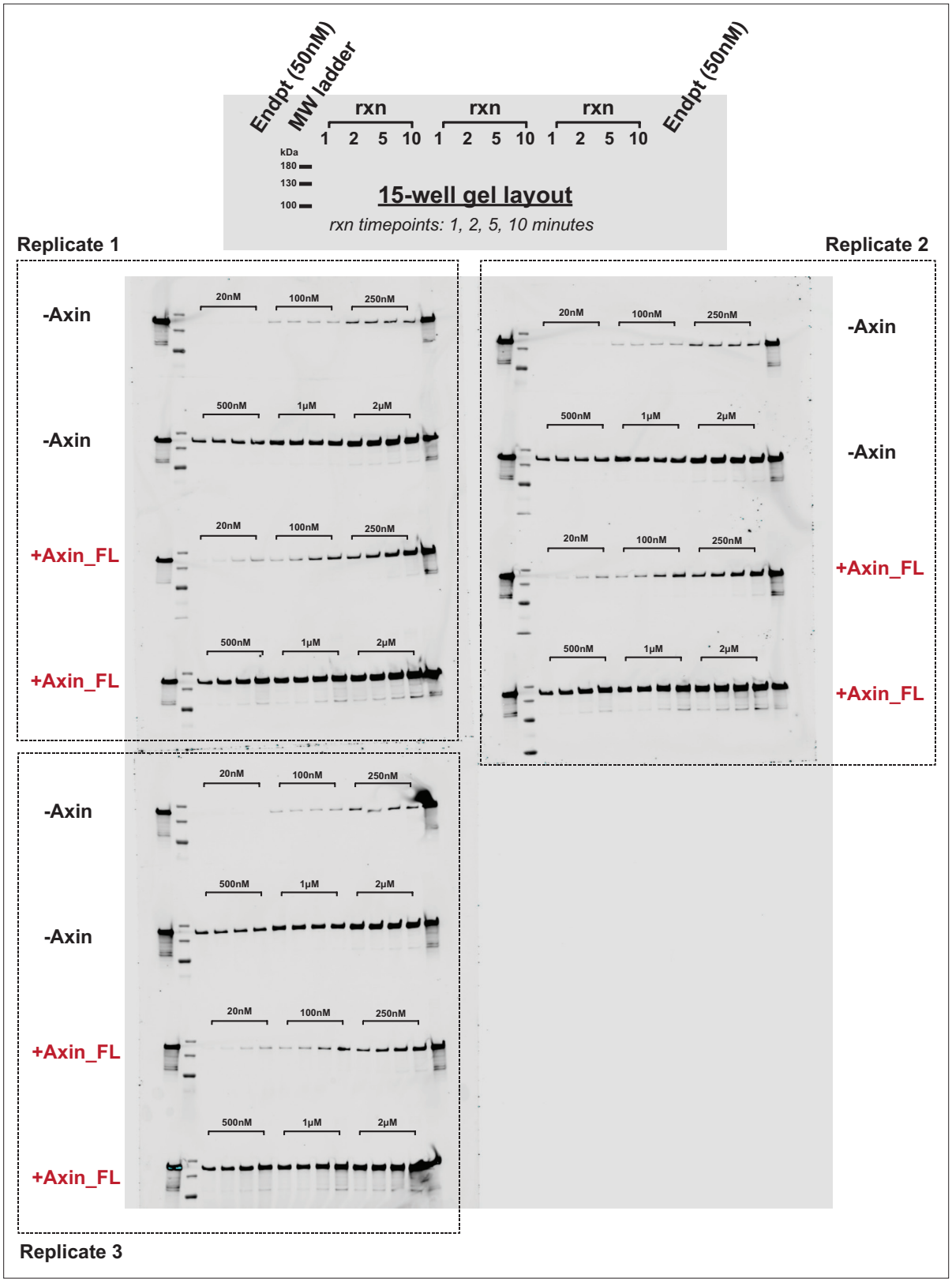

Figure 2—figure supplement 6. Representative western blots for the reaction of pS9-GSK3β with pS45-β-catenin in the presence and absence of Axin. Western blots for reactions of varying concentrations of pS45-β-catenin with 10 nM pS9-GSK3β in the presence and absence of 500 nM Axin. All gel samples were diluted 1:5 to prevent a gel smearing artifact (see Materials and methods). See ***Figure 2—figure supplement 7*** for quantification.

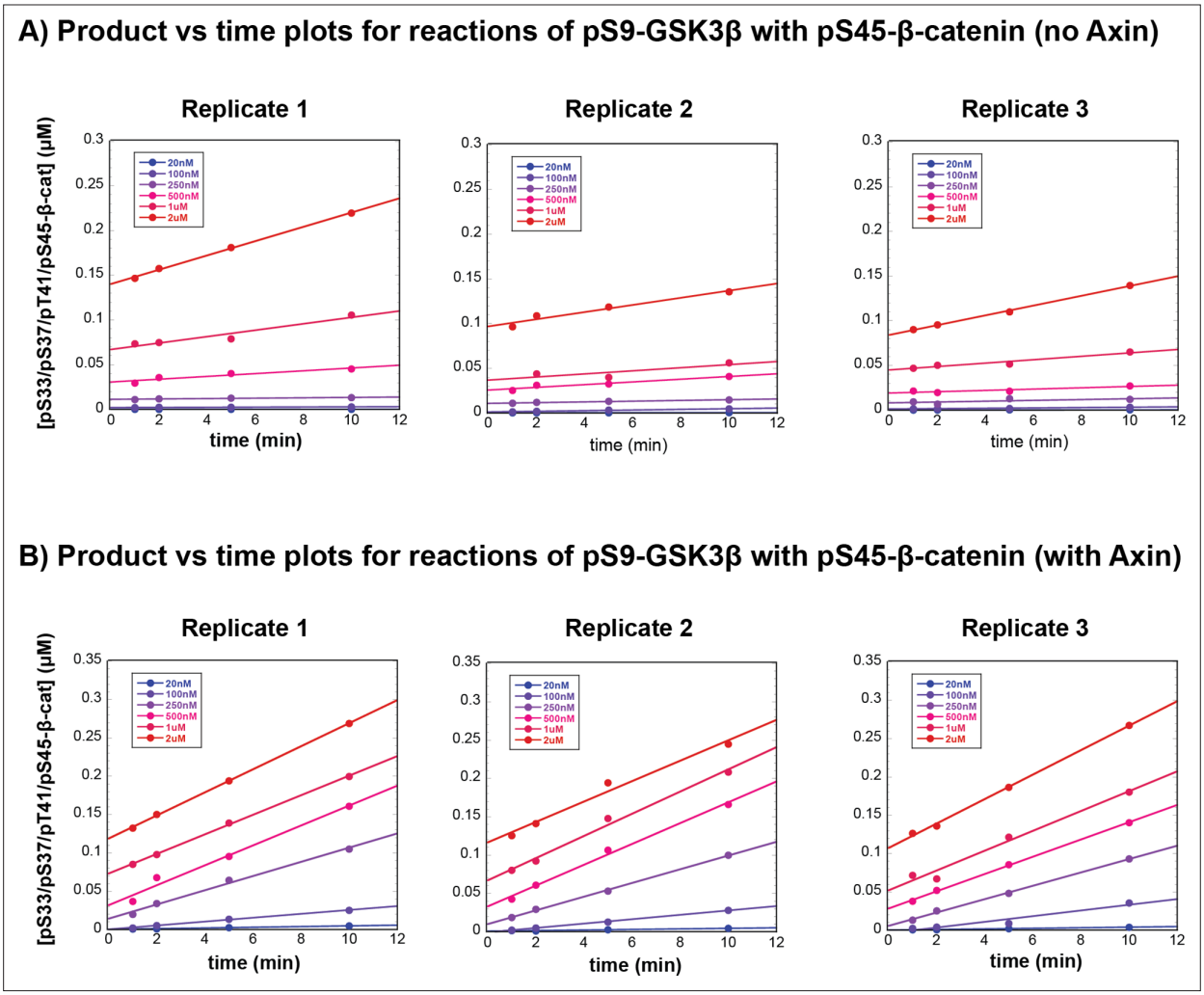

Figure 2—figure supplement 7. Plots of product vs. time for reaction of pS9-GSK3β with pS45-β-catenin in the presence and absence of Axin. (**A**) Product vs. time plots for reactions of pS9-GSK3β with pS45-β-catenin in the absence of Axin. (**B**) Product vs. time plots for reactions of pS9-GSK3β with pS45-β-catenin in the presence of 500 nM Axin. Data in (**A**) and (**B**) correspond to the reaction conditions and western blots shown in ***Figure 2—figure supplement 6***.

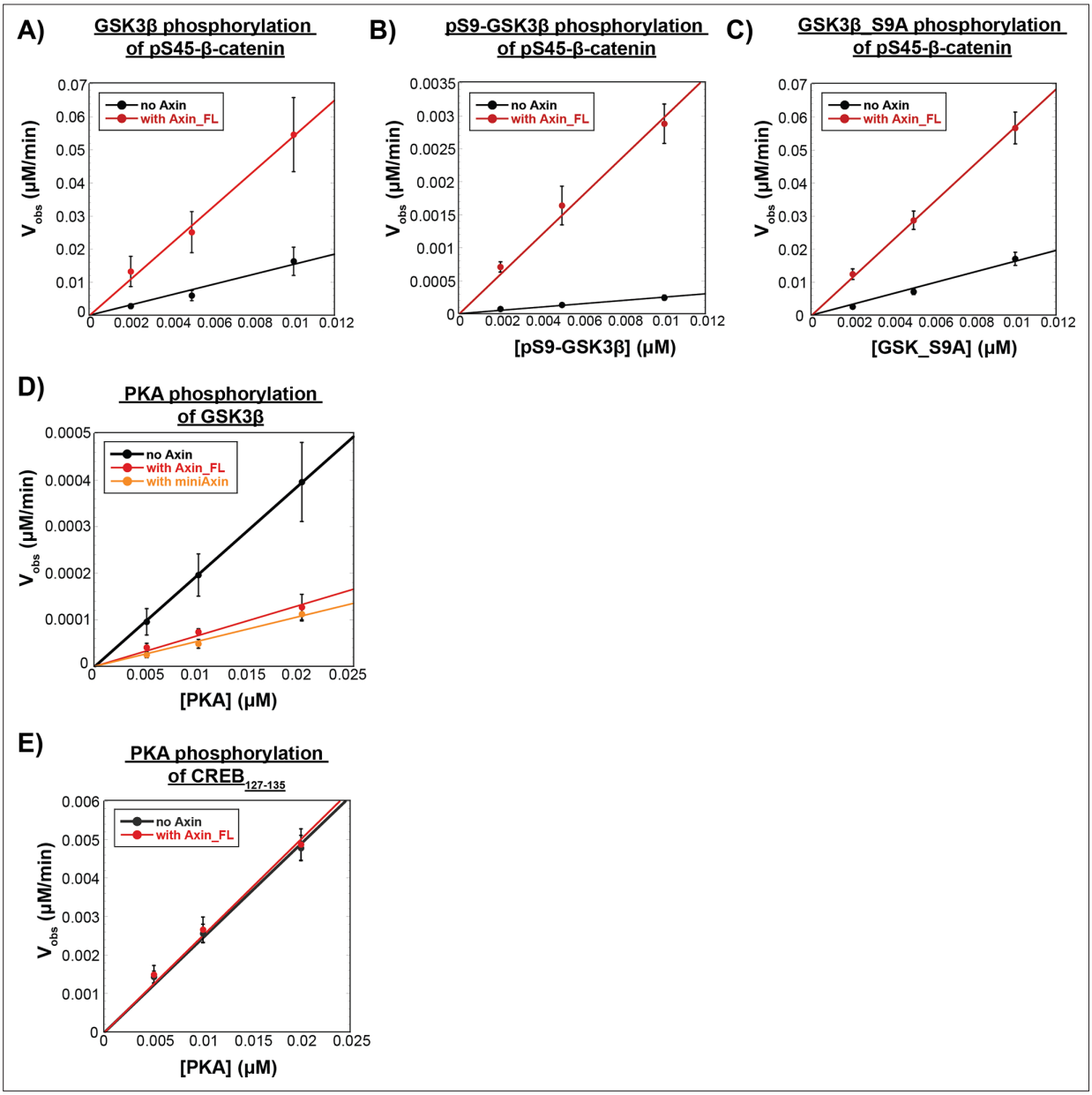

Figure 2—figure supplement 8. V_{obs} vs. [enzyme]. V_{obs} for fixed concentrations of substrate with varying concentrations of GSK3β or PKA in the presence or absence of Axin. (**A**) Plot of V_{obs} vs. [unphosphorylated GSK3β], [pS9-GSK3β], or [GSK3β_S9A] with 50 nM pS45-β-catenin in the presence and absence of 500 nM Axin. V_{obs} increases linearly with enzyme concentration, as expected. (**B**) Plot of V_{obs} vs. [pS9-GSK3β] with 50 nM pS45-β-catenin in the presence and absence of 500 nM Axin. (**C**) Plot of V_{obs} vs. [GSK3β_S9A] with 50 nM pS45-β-catenin in the presence and absence of 500 nM Axin. (**D**) Plot of V_{obs} vs. [PKA] with 20 nM GSK3β in the presence and absence of 500 nM Axin_FL or miniAxin. (**E**) Plot of V_{obs} vs. [PKA] at 20 nM $CREB_{127-135}$ in the presence and absence of 500 nM Axin. Error bars are mean ± SD for at least three biological replicates.

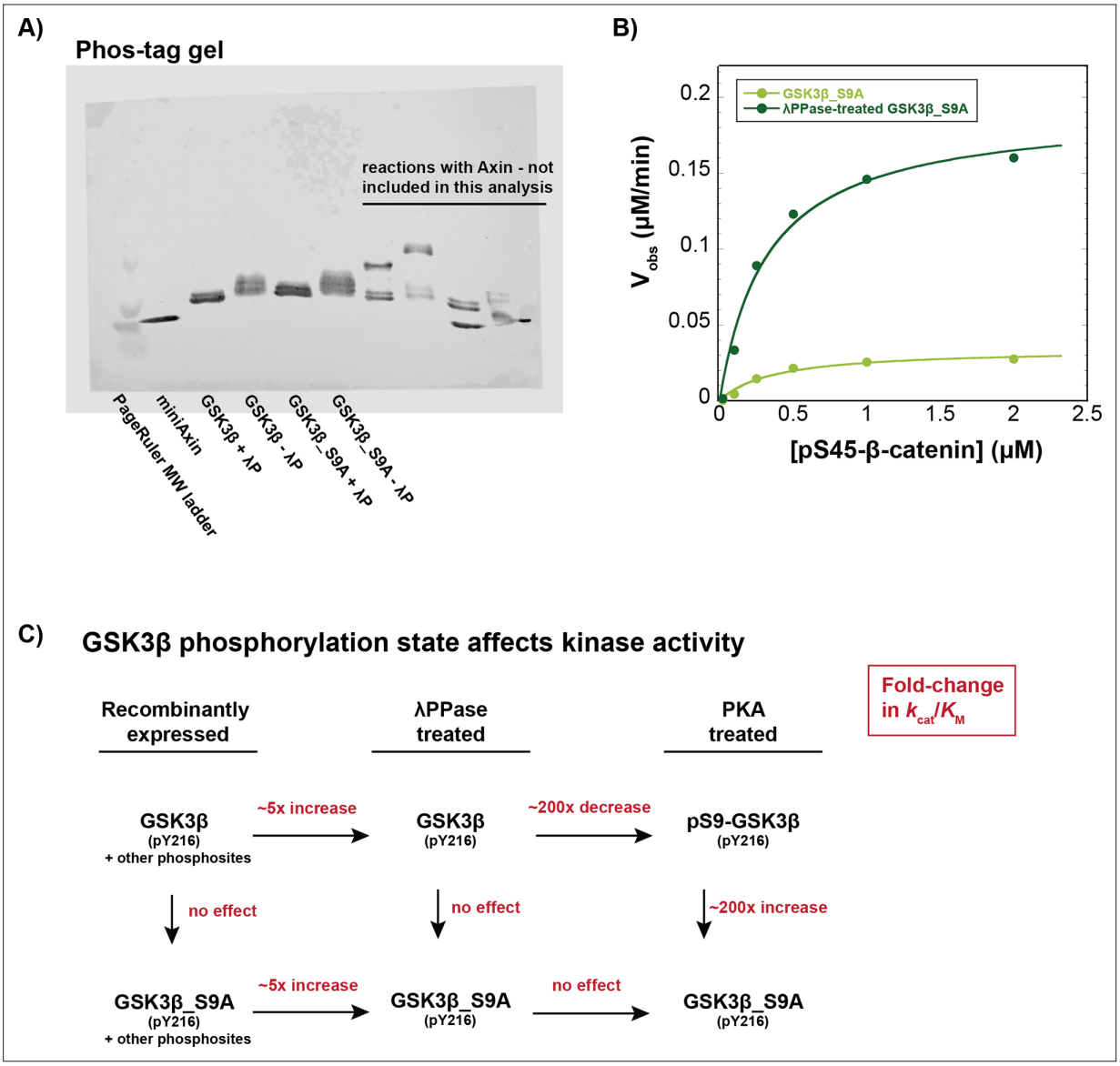

Figure 2—figure supplement 9. Recombinant GSK3β is phosphorylated on multiple sites. (**A**) Recombinant GSK3β is phosphorylated at phosphosites other than Ser9. Phos-tag gel of GSK3β and GSK3β_S9A with and without treatment with lambda phosphatase. Phos-tag gels were prepared and run as previously described (***Gavagan et al., 2020***; see Materials and methods). Samples with GSK3β or GSK3β_S9A were prepared in PMP buffer (NEB) with 1 mM $MnCl_2$ and 400 nM GSK3β or GSK3β_S9A and incubated in the presence or absence of 30 μM lambda phosphatase for 30 min at 30 °C. The slower-migrating species are phosphorylated GSK3β or GSK3β_S9A. The presence of phosphorylated bands in GSK3β_S9A indicates that additional sites besides Ser9 are phosphorylated in recombinant GSK3β. (**B**) Michaelis-Menten plot of V_{obs} versus [pS45-β-catenin] at 10 nM GSK3β_S9A or 10 nM lambda phosphatase-treated GSK3β_S9A. Dephosphorylation of GSK3β_S9A by lambda phosphatase produces an ~5 fold increase in k_{cat}/K_M, largely due to a ~fivefold increase in k_{cat}. See ***Supplementary file 1d*** for values of fitted kinetic parameters. (**C**) GSK3β kinase activity is affected by phosphorylation state at Ser9 and other phosphosites. Values on arrows are fold-change in k_{cat}/K_M for different preparations of GSK3β in reactions with pS45-β-catenin. Dephosphorylation of wt GSK3β or GSK3β _S9A by lambda phosphatase produces ~fivefold increases in k_{cat}/K_M (***Supplementary file 1e***). PKA phosphorylation of lambda phosphatase-treated GSK3β to produce pS9-GSK3β leads to a ~200-fold decrease in k_{cat}/K_M (***Figure 2***, ***Supplementary file 1a and e***). PKA phosphorylation of lambda phosphatase-treated GSK3β_S9A produces no effect on k_{cat}/K_M because GSK3β_S9A cannot be phosphorylated at the inhibitory Ser9 phosphosite (***Figure 2***, ***Supplementary file 1e***).

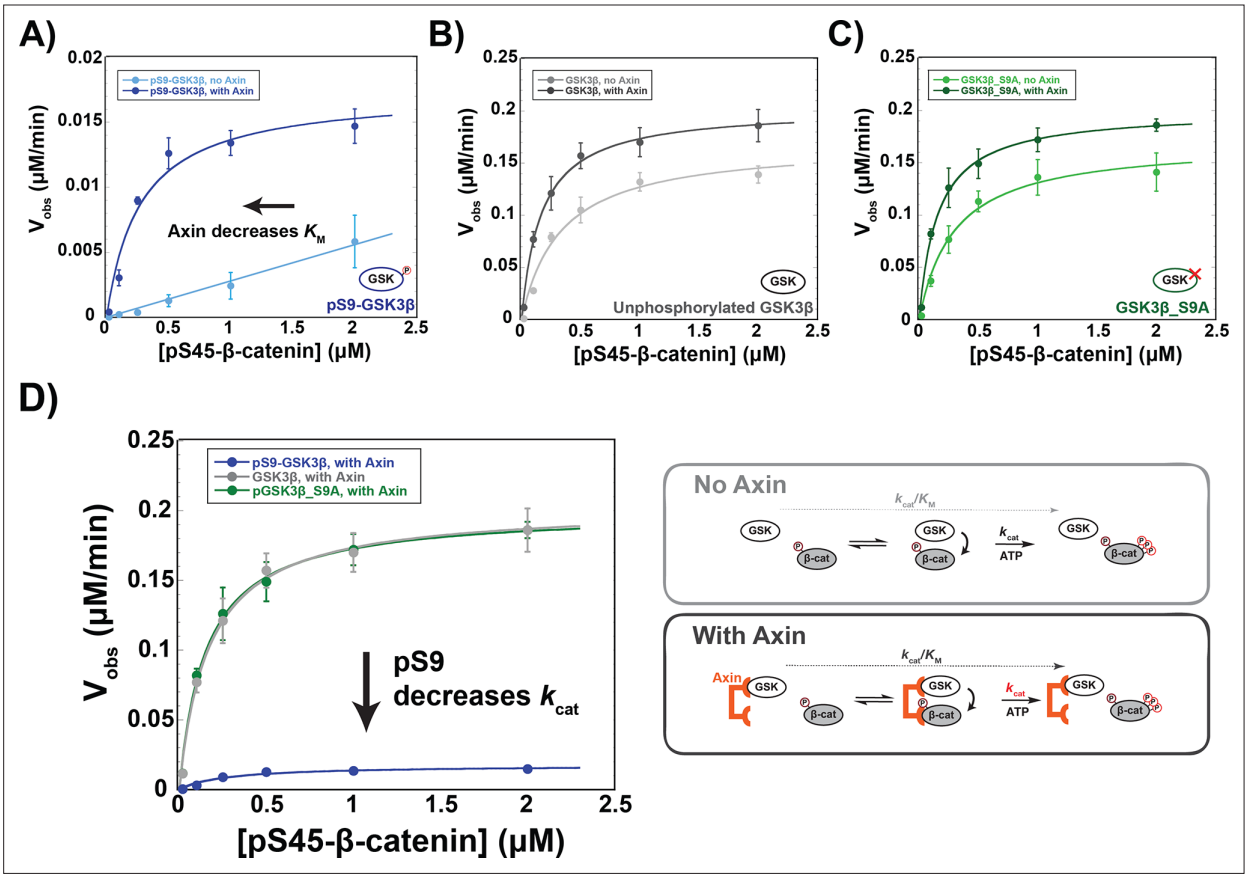

Figure 3. Axin restores the K_M for β-catenin but cannot overcome pS9-GSK3β inactivation. (**A–C**) Michaelis-Menten plots of V_{obs} versus [pS45-β-catenin] in the presence and absence of 500 nM Axin with 10 nM pS9-GSK3β (**A**), unphosphorylated GSK3β (**B**) or PKA-treated GSK3β_S9A (**C**). At the Axin concentrations used in these experiments all the GSK3β is bound to Axin (***Gavagan et al., 2020***). (**D**) Minimal kinetic scheme and Michaelis-Menten plots for reactions of GSK3β with pS45-β-catenin in the presence of Axin plotted on the same scale. Values are mean ± SD for at least three biological replicates. See ***Supplementary file 1a*** for values of fitted kinetic parameters.

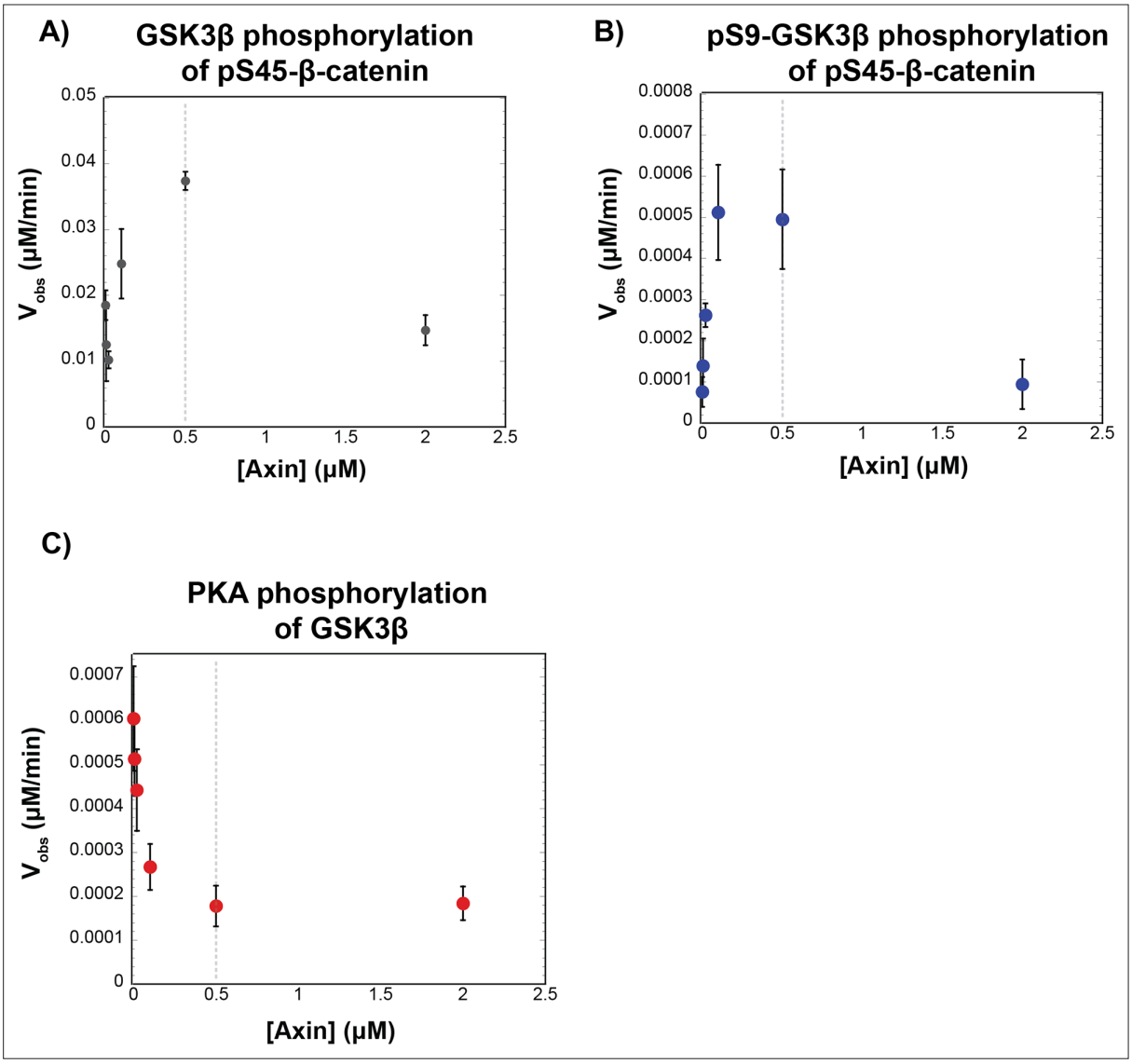

Figure 3—figure supplement 1. Varying the concentration of Axin does not produce larger rate effects than observed with 500 nM Axin. (**A**) Plots of V_{obs} vs. [Axin] with 10 nM unphosphorylated GSK3β and 50 nM pS45-β-catenin. (**B**) Plots of V_{obs} vs. [Axin] with 10 nM pS9-GSK3β and 50 nM pS45-β-catenin. (**C**) Plots of V_{obs} vs. [Axin] with 20 nM PKA and 20 nM GSK3β. Error bars are mean ± SD for at least three biological replicates.

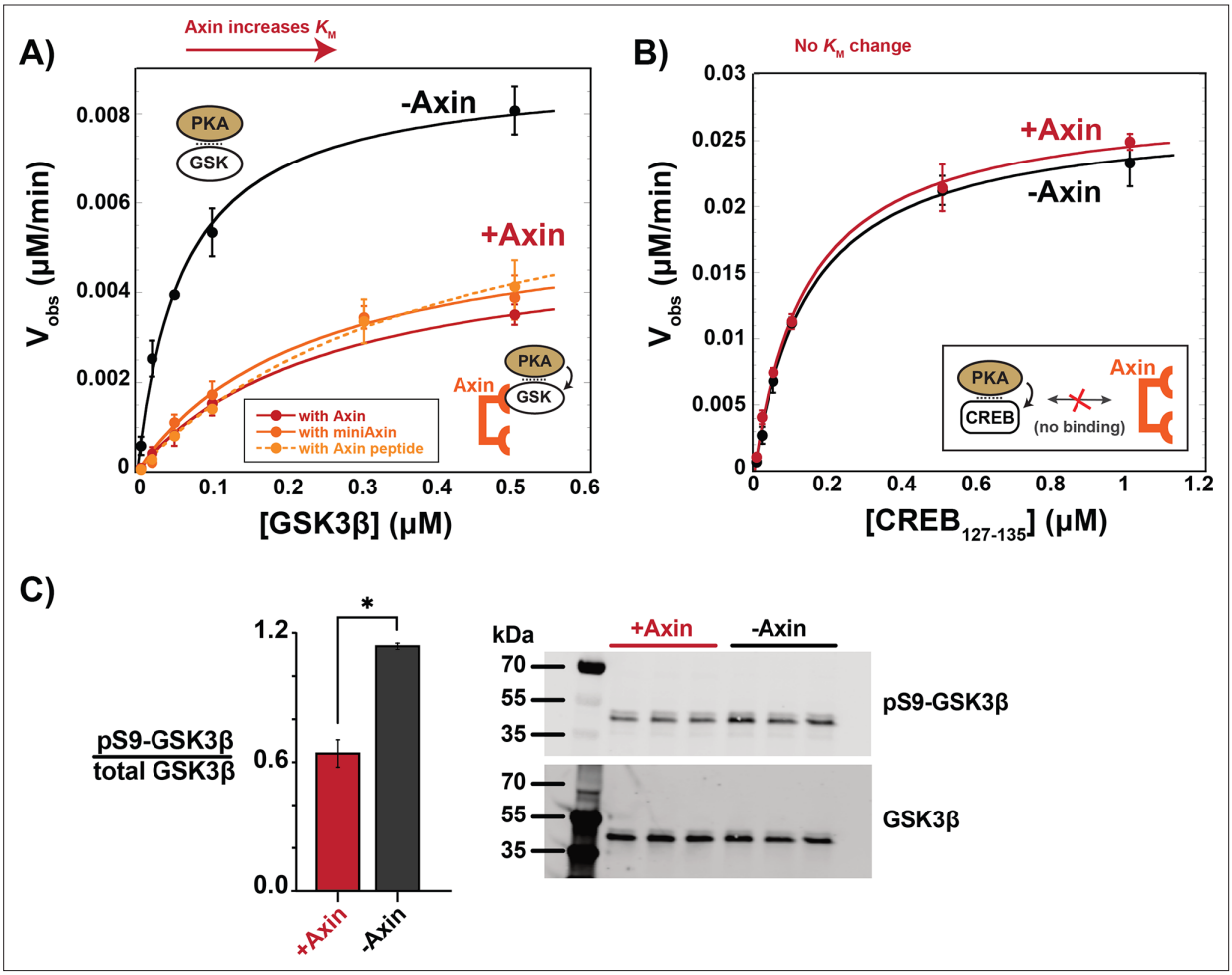

Figure 4. Axin prevents phosphorylation of GSK3β at Ser9. (**A**) Michaelis-Menten plots of V_{obs} versus [GSK3β] with 20 nM PKA in the presence and absence of 500 nM Axin. (**B**) Michaelis-Menten plots of V_{obs} versus [CREB$_{127-135}$] with 20 nM PKA in the presence and absence of 500 nM Axin. Values are mean ± SD for at least three biological replicates. See ***Supplementary file 1b*** for values of fitted kinetic parameters from (**A**) and (**B**). (**C**) Normalized western blot analysis and blot images of pS9-GSK3β in HEK293 cells transiently expressing Axin or a negative control (see Materials and methods). Normalized pS9-GSK3β levels were calculated for each biological sample by dividing pS9-GSK3β signal by total GSK3β and then averaging across three biological replicates. The p-value between Axin-expressing cells and non-Axin negative control cells is 0.00356 (two-tailed unpaired t-test). Full, uncropped western blot images are shown in ***Figure 4—figure supplement 3***.

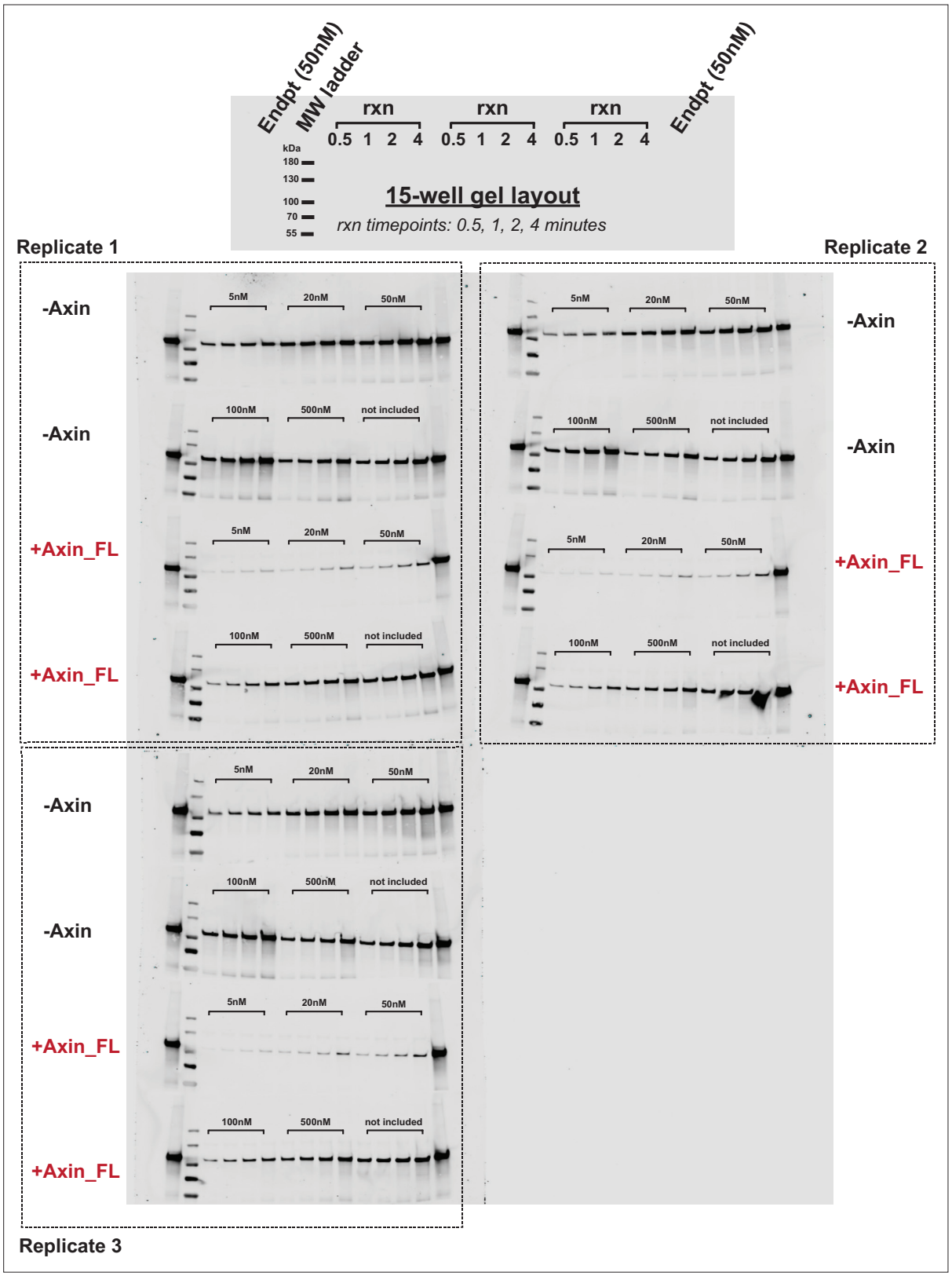

Figure 4—figure supplement 1. Representative western blots for the reaction of PKA with GSK3β in the presence and absence of Axin. Western blots for reactions of varying concentrations of GSK3β with 20 nM PKA +/-500 nM Axin. 500 nM GSK3β reaction gel samples without Axin were diluted 1:4 to prevent overloading the gel; all other reactions were diluted 1:2 (see Materials and methods). See ***Figure 4—figure supplement 2*** for quantification.

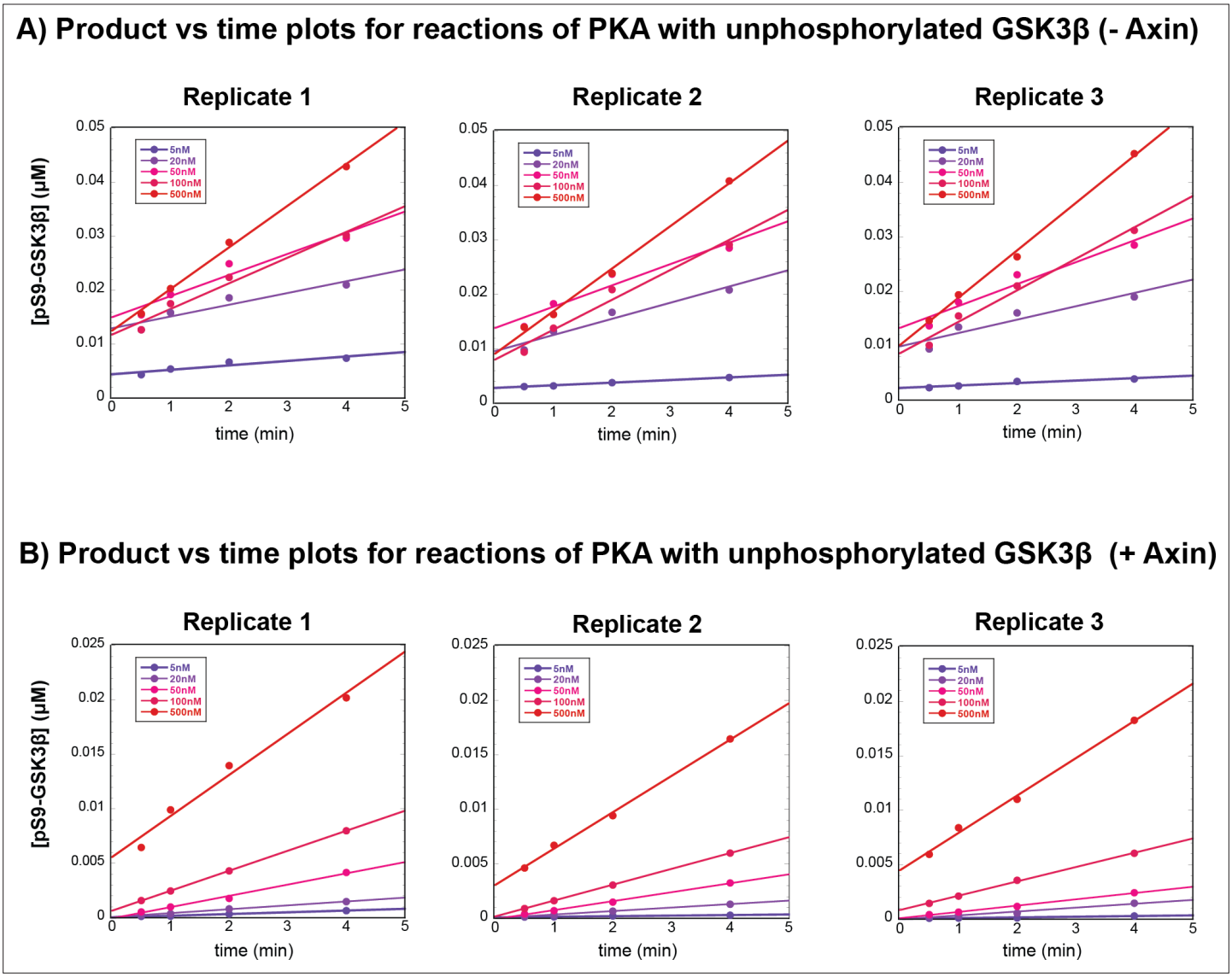

Figure 4—figure supplement 2. Plots of product vs. time for reaction of PKA with GSK3β in the presence and absence of Axin. (**A**) Product vs. time plots for reactions of PKA with GSK3β in the absence of Axin. (**B**) Product vs. time plots for reactions of PKA with GSK3β in the presence of 500 nM Axin. Data in (**A**) and (**B**) correspond to the reaction conditions and western blots shown in ***Figure 4—figure supplement 1***.

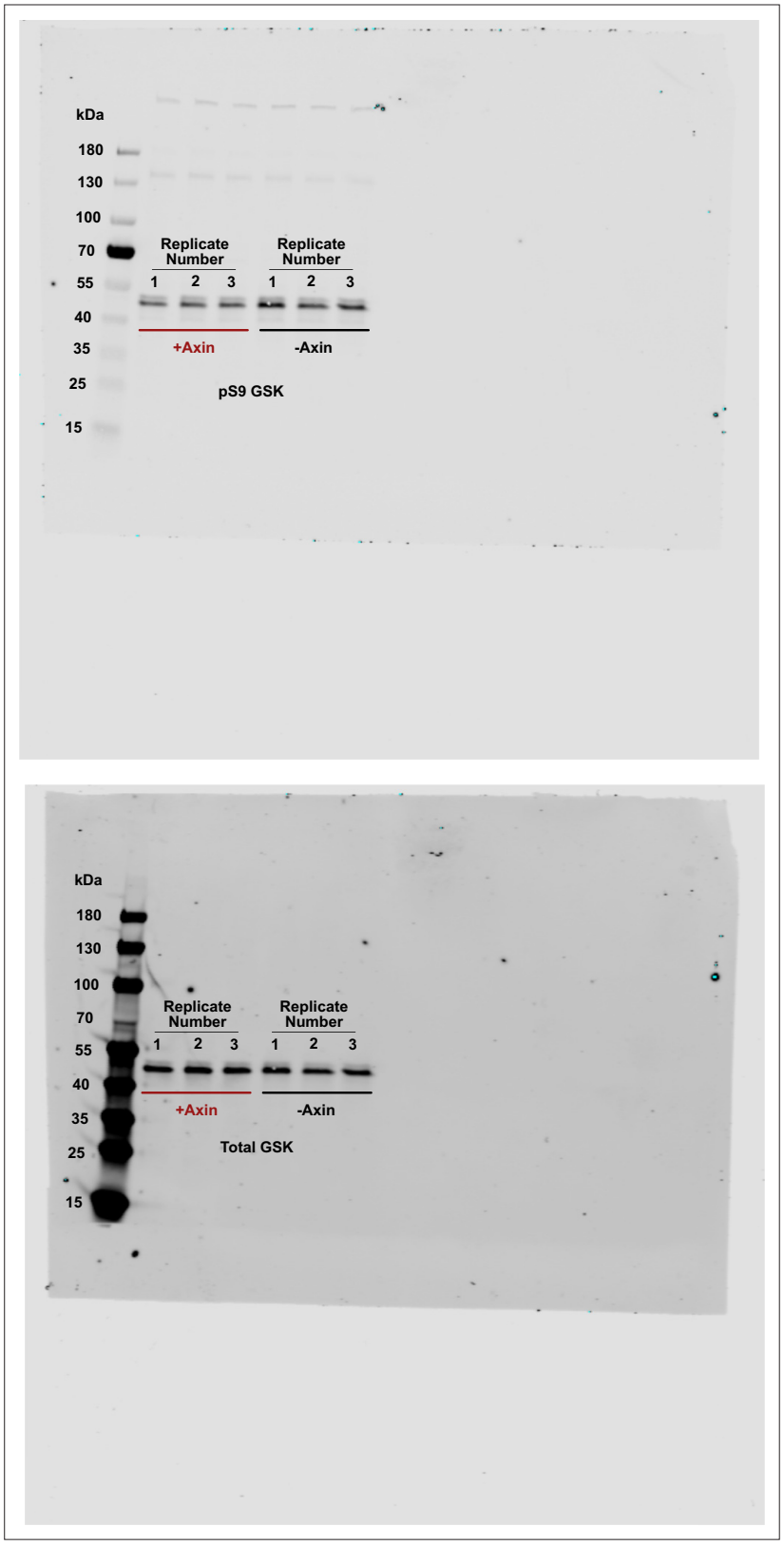

Figure 4—figure supplement 3. Uncropped western blots for pS9-GSK3β in HEK293 cells. Western blot images of pS9-GSK3β and total GSK3β in HEK293 cells transiently expressing Axin or a negative control.

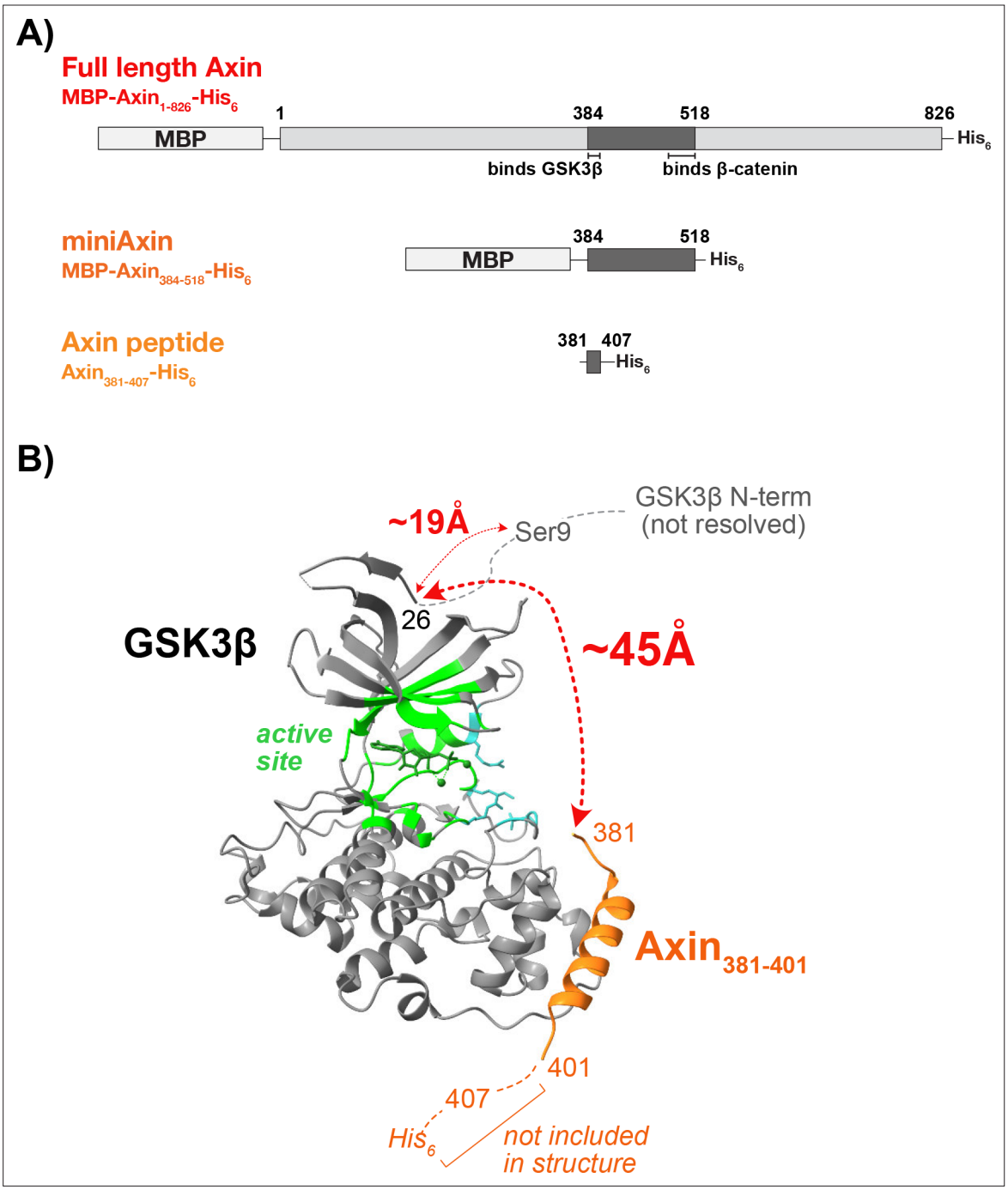

Figure 4—figure supplement 4. The Axin peptide is too far from the N-terminus of GSK3β to sterically occlude the Ser9 phosphorylation site. (**A**) Schematics of full length Axin, miniAxin, and the minimal Axin peptide used in functional studies. Full length Axin and miniAxin were purified with an N-terminal maltose binding protein (MBP) and a C-terminal His tag. The Axin peptide was expressed as an MBP fusion and cleaved with TEV protease to produce the minimal sequence GS-$Axin_{381-407}$-SGR-His_6 (see Methods). (**B**) Crystal structure of GSK3β in complex with $Axin_{381-401}$ (pdb 4nm0, ***Stamos et al., 2014***). The GSK3β N-terminal residues 1–25 are not resolved. The Cα-Cα distance from Axin Ile381 to GSK3β Met26 is ~45 Å along the surface of GSK3β, determined by manually plotting five possible paths from Cα-Cα along the surface of GSK3β with distances of 48.1 Å, 44.7 Å, 45.4 Å, 49.9 Å, and 44.3 Å. For example, one path was calculated by measuring and summing the distances between the Cα of Met26 on GSK3β to the Cα of Lys123 on GSK3β and from the Cα of Lys123 on GSK3β to the Cα of Ile381 on Axin. These estimates are likely conservative, as we did not consider steric clash with GSK3β side chains. The direct linear Cα-Cα distance from Axin Ile381 to GSK3β Met26 is 41 Å, but this path sterically clashes with the N-lobe of the kinase. To estimate the distance of ~19 Å from GSK3β Met26 to Ser9, we used a worm-like chain model for a flexible peptide (***Bertagna et al., 2008***). Therefore, the minimal $Axin_{381-407}$ peptide is unlikely to sterically occlude access to Ser9. Molecular graphics and analyses performed with UCSF Chimera, developed by the Resource for Biocomputing, Visualization, and Informatics at the University of California, San Francisco, with support from NIH P41-GM103311 (***Pettersen et al., 2004***).